

Q-Diffusion: Quantizing Diffusion Models

Xiuyu Li
UC Berkeley

Long Lian
UC Berkeley

Yijiang Liu
Nanjing University

Huanrui Yang
UC Berkeley

Zhen Dong
UC Berkeley

Daniel Kang
UC Berkeley

Shanghang Zhang
Peking University

Kurt Keutzer
UC Berkeley

Abstract

Diffusion models have recently achieved great success in synthesizing diverse and high-fidelity images. However, sampling speed and memory constraints remain a major barrier to the practical adoption of diffusion models as the generation process for these models can be slow due to the need for iterative noise estimation using complex neural networks. We propose a solution to this problem by compressing the noise estimation network to accelerate the generation process using post-training quantization (PTQ). While existing PTQ approaches have not been able to effectively deal with the changing output distributions of noise estimation networks in diffusion models over multiple time steps, we are able to formulate a PTQ method that is specifically designed to handle the unique multi-timestep structure of diffusion models with a data calibration scheme using data sampled from different time steps. Experimental results show that our proposed method is able to directly quantize full-precision diffusion models into 8-bit or 4-bit models while maintaining comparable performance in a training-free manner, achieving a FID change of at most 1.88. Our approach can also be applied to text-guided image generation, and for the first time we can run stable diffusion in 4-bit weights without losing much perceptual quality, as shown in Figure 5 and Figure 9.

1. Introduction

Diffusion models showed great success in generating images that are both diverse and high-fidelity [42, 17, 43, 41, 9, 32, 35, 34]. Recent work [20, 18] has demonstrated superior performance than state-of-the-art GAN models, which suffer from unstable training. With their flexibility on downstream tasks, diffusion models demonstrate their power in various applications such as image super-resolution [36, 23], inpainting [43], shape generation [5], graph generation [31],

image-to-image translation [39], and molecular conformation generation [46].

However, the generation process for diffusion models can be slow due to the need for iterative noise estimation using complex neural networks at each time step, creating obstacles for deployment, particularly on edge devices. The inference normally requires 50 to 1,000 denoising time steps [17, 41], and has high memory consumption. It normally takes several seconds for diffusion models to sample a single image, while previous state-of-the-art approaches (e.g. GANs) are able to generate multiple images in under 1 second. Consequently, it is in need to speed up their generation process and reduce the memory requirements.

There are two major factors that slow down the denoising process: the repeating process of sampling images from noise through multiple iterations, and the complex network used to estimate noise in each iteration. Previous work has attempted to accelerate the first factor by finding shorter, more effective sampling trajectories [7, 41, 33, 1, 27, 38]. Nevertheless, these approaches do not address the issue of the time-consuming noise estimation process in each iteration of neural network inference.

In contrast, our work tackles the second factor, where we focus on compressing and accelerating the noise estimation model, i.e. UNet, used in the diffusion denoising process. Among previously explored compression methods, the extensive shortcut connections of UNet models lead to complex dimensionality constraints across multiple layers, which requires significant engineering effort to find valid structure via pruning [48, 40] or neural architecture search [4]. Quantization compresses the model without modifying the model architecture. However, the commonly used quantization-aware training [51, 11, 47, 10, 45] retrains the model at low precision, which may be unstable given the complicated training scheme of diffusion models, and are constrained by the lack of public training data [32, 35]. Therefore, we find the training-free post-training quantiza-

tion (PTQ) [6, 2, 24, 15, 26] the most applicable for diffusion model compression.

In this work, we propose a solution to leverage PTQ to compress the cumbersome noise estimation network in diffusion models in a data-free, training-free manner, while maintaining comparable performance to the full precision counterparts. Our work provides the first thorough analysis of the novel challenges of performing PTQ on diffusion model. Specifically, we discover that the output distribution of the noise estimation network at each time step can be largely different, and naively applying previous PTQ approaches with an arbitrary time step leads to poor performance. Furthermore, the distinctive UNet architecture used by diffusion models requires special design on the quantization scheme and calibration objectives. We propose a novel data sampling and calibration scheme for diffusion models, which automatically selects the time steps and determines the number of samples drawn from each time step to form a calibration set that corrects the quantizer functions in diffusion models. We further analyze the sensitivity of UNet architecture to quantization and adjust our quantization scheme accordingly for the best efficiency-accuracy trade-off. The contributions of this paper can be summarized as follows:

1. We perform a thorough analysis of the weight and activation distribution in the granularity of time steps and layers, showcasing the challenges of performing PTQ on diffusion models.
2. We propose a cross-time step calibration data sampling method for diffusion model PTQ to balance the calibration quality and the dataset size.
3. Our proposed method enables W4A8 PTQ for both pixel-space and latent-space diffusion models with a FID increment of only 0.39-1.88, and can produce qualitatively comparable samples when being applied on Stable Diffusion for text-guided image synthesis.

2. Background

Image Synthesis Image synthesis aims to generate synthetic images that follow the distribution of real images. Deep generative models have made great progress in image synthesis in recent years. Among them the most popular types of generative models are variational auto-encoder (VAE) [21], flow-based models, generative adversarial networks (GAN) [14], and diffusion-based models [42, 17]. GANs have dominated the field of image synthesis for years [3, 19, 20, 18] before recently diffusion models [9, 34, 32, 35] are shown to perform on par or better than state-of-the-art GANs with more stable training procedures and can be applied to a wide range of modalities.

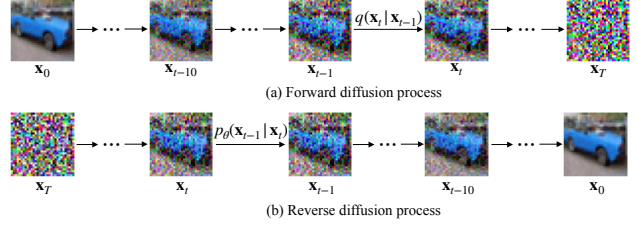


Figure 1: The forward diffusion process (a) repeatedly adds Gaussian noise. The reverse diffusion process (b) uses a trained network to denoise from a standard Gaussian noise image in order to generate an image. Note that the samples between two consecutive time steps (e.g., time step $t - 1$ and time step t) are very similar, but samples in relatively distant time steps do have substantially different noise levels.

Diffusion Models Diffusion models model the image generation process with a series of steps on a Markov chain. During the forward diffusion process, each step adds noise to the data, eventually making the data follow a standard normal distribution. The reverse process removes noise from the data, which is leveraged to gradually generate high-fidelity images from standard Gaussian noise. See Figure 1 for a graphical illustration. We refer readers to [29] for a more detailed introduction.

Let \vec{x}_0 be a sample from the data distribution $\vec{x}_0 \sim q(\vec{x})$. A forward diffusion process adds Gaussian noise to the sample for T times, resulting in a sequence of noisy samples $\vec{x}_1, \dots, \vec{x}_T$:

$$q(\vec{x}_t | \vec{x}_{t-1}) \sim \mathcal{N}(\sqrt{1 - \beta_t} \vec{x}_{t-1}, \beta_t \mathbf{I}) \quad (1)$$

where $\beta_t \in (0, 1)$ is the variance schedule and controls the strength of the Gaussian noise in each step.

Since each step only depends on the one previous step, the forward diffusion process follows Markov property. Furthermore, when $T \rightarrow \infty$, \vec{x}_T approaches an isotropic Gaussian distribution.

Diffusion models generate a sample from a Gaussian noise input $\vec{x}_T \sim \mathcal{N}(\vec{0}, \mathbf{I})$ by reversing the forward process. However, since the real reverse conditional distribution $q(x_{t-1} | x_t)$ is unavailable to us, diffusion models sample from a learned conditional distribution $p_\theta(x_{t-1} | x_t)$ which approximates the real reverse conditional distribution with a Gaussian distribution:

$$p_\theta(\vec{x}_{t-1} | \vec{x}_t) = \mathcal{N}(\vec{x}_{t-1}; \tilde{\mu}_{\theta,t}(\vec{x}_t), \tilde{\beta}_t \mathbf{I}) \quad (2)$$

With the reparameterization trick in [17], the mean $\tilde{\mu}_{\theta,t}(\vec{x}_t)$ and variance $\tilde{\beta}_t$ could be derived:

$$\tilde{\mu}_{\theta,t}(\vec{x}_t) = \frac{1}{\sqrt{\alpha_t}} \left(\mathbf{x}_t - \frac{1 - \alpha_t}{\sqrt{1 - \bar{\alpha}_t}} \vec{\epsilon}_{\theta,t} \right) \quad (3)$$

$$\tilde{\beta}_t = \frac{1 - \bar{\alpha}_{t-1}}{1 - \bar{\alpha}_t} \cdot \beta_t \quad (4)$$

where $\alpha_t = 1 - \beta_t$, $\bar{\alpha}_t = \prod_{i=1}^t \alpha_i$.

At training time, the goal of optimization is to minimize the negative log-likelihood $-\log p_\theta(\mathbf{x}_0)$. With variational inference, a lower bound of it could be found, denoted as L_{VLB} :

$$L_{\text{VLB}} = \mathbb{E}_{q(\vec{x}_{0:T})} [\log \frac{q(\vec{x}_{1:T}|\vec{x}_0)}{p_\theta(\vec{x}_{0:T})}] \geq -\log p_\theta(\vec{x}_0) \quad (5)$$

It is found in [17] that using a simplified loss function to L_{VLB} often obtains better performance:

$$L_t^{\text{simple}} = \mathbb{E}_{t \sim [1, T], \vec{x}_0, \vec{\epsilon}_t} [\|\vec{\epsilon}_t - \tilde{\epsilon}_\theta(\sqrt{\bar{\alpha}_t}\vec{x}_0 + \sqrt{1 - \bar{\alpha}_t}\vec{\epsilon}_t, t)\|^2] \quad (6)$$

At inference time, a Gaussian noise tensor \vec{x}_T is sampled and is denoised by repeatedly sampling the reverse distribution $p_\theta(\vec{x}_{t-1}|\vec{x}_t)$. $\tilde{\mu}_{\theta,1}(\vec{x}_1)$ is taken as the final generation result, with no noise added in the final denoising step.

Post-training Quantization In situations with limited training data or computing resources for the time-consuming quantization-aware fine-tuning process [49], post-training quantization (PTQ) becomes a preferred method of quantization. Most previous works [13] use the rounding-to-nearest approach, which quantizes deep neural networks by rounding elements w to the nearest quantization values. The quantization and dequantization can be formulated as:

$$\hat{w} = s \cdot \text{clip}(\lfloor \frac{w}{s} \rfloor, c_{\min}, c_{\max}) \quad (7)$$

where s denotes the quantization scale parameters, c_{\min} and c_{\max} are the lower and upper bounds for the clipping function $\text{clip}(\cdot)$. The operator $\lfloor \cdot \rfloor$ represents rounding-to-nearest.

Researchers have previously focused on using PTQ with convolutional neural networks (CNNs). For example, EasyQuant [44] presents an efficient method to determine appropriate clipping ranges for quantization, and ZeroQ [6] employs a distillation technique to generate proxy input images for PTQ, which utilizes the inherent statistics of batch normalization layers. SQuant [15] adjusts the model to reduce quantization error based on sensitivity determined through the Hessian spectrum. BRECQ [24] introduces Fisher information into the objective, and optimizes layers within a single residual block jointly using a small subset of calibration data from the training dataset. Some of the PTQ methods still need training datasets to calibrate quantized models [30, 24] but are often unavailable due to privacy and commercial reasons, such as medical and confidential scenarios. Fortunately, in the quantization of diffusion models, the calibration dataset can be constructed by sampling the full precision model, as the input for the denoising process is always gaussian noise (with some user-defined conditions in the conditional generation scenarios). Given the diffusion

models are fully trained to convergence, it is reasonable to assume that the sampled data distribution will be a nearly exact match to the training data distribution, enabling the creation of a high-quality calibration dataset in a zero-shot manner. This further shows that post-training quantization is a well-suited method for accelerating diffusion models.

3. Method

This Section proposes the method for Diffusion Model post-training quantization. Different from conventionally studied deep learning models and tasks (e.g. CNNs, VITs for image classification, or object detection), Diffusion Models are trained and evaluated in a distinctive multi-step manner. This draws notable challenges to the PTQ process. We analyze the challenge brought by the multi-step inference process in Section 3.1, and describe the full PTQ pipeline in Section 3.2.

3.1. Challenges under the Multi-step Denoising

Here we identify two major challenges on PTQ specific to the multi-step inference process of Diffusion Models. Namely, we investigate on the accumulation of quantization error, and the difficulty of sampling a small calibration dataset to reduce the quantization error.

Challenge 1: Quantization errors accumulate across time steps. Performing quantization on a neural network model introduces noises on the weight and activation of the well-trained model, leading to quantization errors in each layer’s output. Previous research has identified that quantization errors are likely to accumulate across layers [8], making deeper neural networks harder to quantize. In the case of Diffusion Models, at any time step t , the input of the denoising model (denote as x_t) is derived by x_{t+1} , the output of the model at the previous time step $t + 1$ (as depicted by Equation 2). This process effectively multiplies the number of layers involved in the computation by the number of denoising steps for the input x_t at time step t , leading to an accumulation of quantization errors towards later steps in the denoising process.

We run the denoising process of DDIM [41] on CIFAR10 with a sampling batch size of 64, and compare the MSE differences between the full precision model and the model quantized to INT8, INT5, and INT4 at each time step. As shown in Figure 2, there is a dramatic increase in the quantization errors when the model got quantized to 4-bit, and the errors accumulate quickly through iterative denoising. This brings difficulty in preserving the performance after quantizing the model down to low precision, which requires the reduction of quantization error at all time steps as much as possible.

Challenge 2: Activation distributions vary across time steps. To reduce the quantization error at each time step,

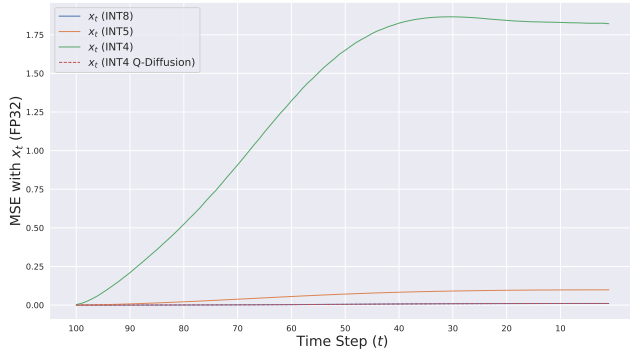


Figure 2: MSE between FP32 outputs and weight-quantized outputs of different precisions with Linear Quantization and our approach across time steps. Here the data is obtained by passing a batch with 64 samples through a model trained on CIFAR-10 with DDIM sampling steps 100.

we follow the common practice in PTQ research [30, 24] to calibrate the clipping range and scaling factors of the quantized model with a small set of calibration data. The calibration data should be sampled to resemble the true input distribution so that the activation distribution of the model can be estimated correctly for proper calibration. Given that the Diffusion Model takes input from all time steps, determining the data sampling policy across different time steps becomes an outstanding challenge. Here we start by analyzing the output activation distribution of each layer in the UNet model across different time steps. We conduct the same CIFAR10 experiment using DDIM with 100 denoising steps, and draw the activations ranges of 1000 random samples among all time steps. As Figure 3 shows, the activation distributions gradually change, with neighboring time steps being similar and distant ones being distinctive.

The fact that output activations distribution across time steps are not always the same further brings challenges to quantization. Calibrating the UNet model using a single time step will cause overfitting to the activation distribution of this specific time step, while not generalizing to other time steps. For instance, here we try to calibrate the quantized DDIM on the CIFAR10 dataset with the commonly used BRECQ [24] method, and compare it with the PTQ model without calibration. As shown in Table 1, if we naively take 5120 samples produced by the denoising process from $t = 0$ for calibration, significant performance drops will be induced under 8-bit and 4-bit weights quantization. The calibrated 8-bit model even performed worse than the naive PTQ model without calibration. This indicates that calibrating with a single time step would lead to significant overfitting and be harmful to the overall performance. In order to recover the performance of the quantized diffusion models, we need to

Method	# W bits	FID↓
Full Precision	32	4.22
No Calibration	8	4.71
Calibrated at $t = 0$	8	10.51
No Calibration	4	141.47
Calibrated at $t = 0$	4	204.76

Table 1: Quantizing DDIM with calibration data sampled from time step $t = 0$.

select calibration data in a way that takes the different time steps outputs distribution into consideration.

3.2. Post-Training Quantization with Timestep-Aware Calibration

In diffusion models inference, the denoising process can be interpreted as a procedure that starts from a sample taken from an isotropic Gaussian distribution, and gradually removes the noise at each time step to recover the corresponding "denoised" image from the training data distribution in the end. This indicates for inputs at nearby consecutive time steps will have a relatively similar distribution, while inputs at distant time steps are distributed more diversely between one another, as illustrated by Figure 1 and Figure 3. With this observation, we randomly sample a few intermediate inputs uniformly in a fixed interval across all time steps to generate a small calibration set, in order to balance the size of the calibration set and its representation ability of the distribution across all time steps. We empirically found that the sampled calibration data is able to recover most of the INT4 quantized models' performance after the calibration, thus adapting this sampling scheme to create the calibration dataset for quantization error correction. Activation functions are kept running at full precision.

To calibrate the quantized model, we divide the model into several reconstruction blocks [24], and iteratively reconstruct outputs and tune the clipping range and scaling factors of weight quantizers in each block with adaptive rounding [30] to minimize the mean squared errors between the quantized and full precision outputs. We define a core component that contains residual connections in the diffusion model UNet as a block, such as a Residual Bottleneck Block or a Transformer Block. Other parts of the model that do not satisfy this condition are calibrated in a per-layer manner. This has been shown to improve the performance to fully layer-by-layer calibration due to better addressing the inter-layer dependencies and generalization [24]. For activation quantization, since activations keep changing over inputs, doing adaptive rounding is infeasible and we only adjust step sizes of quantizers according to [12]. The overall calibration workflow for the quantization is described as follows:

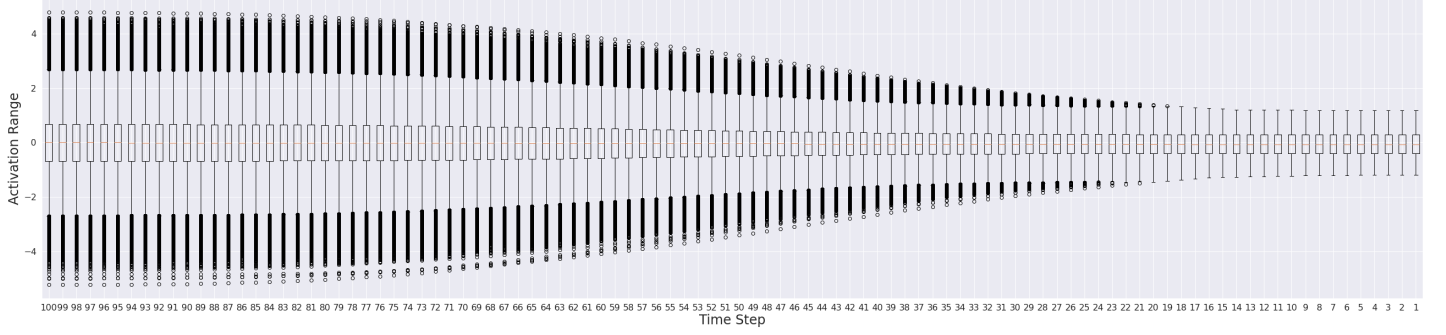


Figure 3: Activation ranges of FP32 outputs across time steps of DDIM model.

Algorithm 1 Q-Diffusion Calibration

Require: Pretrained full precision diffusion model and the quantized diffusion model $[W_\theta, \hat{W}_\theta]$

Require: Empty calibration dataset \mathcal{D}

Require: Number of denoising sampling steps T

Require: Calibration sampling interval c , amount of calibration data per sampling step n

```

for  $t = 1, \dots, T$  time step do
  if  $t \% c = 0$  then
    Sample  $n$  intermediate inputs  $x_t^{(1)}, \dots, x_t^{(n)}$  randomly at  $t$  from  $W_\theta$  and add them to  $\mathcal{D}$ 
  end if
end for
for all  $i = 1, \dots, N$  blocks do
  Update the weight quantizers of the  $i$ -th block in  $\hat{W}_\theta$  with  $\mathcal{D}$  and  $W_\theta$ 
end for
if do activation quantization then
  for all  $i = 1, \dots, N$  blocks do
    Update the activation quantizers step sizes of the  $i$ -th block with  $\hat{W}_\theta, W_\theta, \mathcal{D}$ .
  end for
end if

```

4. Experiments

4.1. Experiments Setup

In this section, we evaluate the proposed Q-Diffusion framework on pixel-space diffusion models (i.e. DDPM [17]) and latent-space diffusion models (i.e. Latent Diffusion [34]) for unconditional image generation. To the best of our knowledge, there is no published work done on diffusion model quantization at this point, so we report channel-wise Linear Quantization (i.e. Equation 7) as a baseline. We further apply our approach to text-guided image synthesis with Stable Diffusion [34]. Experiments show our approach

can achieve competitive generation quality to the full precision scenario on all tasks even under INT4 quantization for weights.

4.2. Unconditional Generation

We conduct evaluation using the 32×32 CIFAR-10 [22], 256×256 LSUN Bedrooms, and 256×256 LSUN Church-Outdoor [50]. We use the pretrained DDIM sampler [41] with 100 denoising time steps for CIFAR-10 experiments, and Latent Diffusion (LDM) [34] for the higher resolution LSUN experiments. The performance is evaluated in FID [16] and Inception Score (IS) [37] for all CIFAR-10 results, while only FID is used for LSUN results as its training data distribution is not like ImageNet, making Inception Score not an accurate reference. We report the results in Table 2- 4 and Figure 4.

Experiments show that Q-Diffusion significantly recovers the image generation quality and significantly outperforms Linear Quantization when the number of bits goes lower for all resolutions and types of diffusion models tested. The 8-bit weight quantization has almost no performance loss to FP32 for both Linear Quantization and our approach due to the high precision. However, the generation quality turns down drastically under 4-bit weight quantization with Linear Quantization, while Q-Diffusion still preserves most of the perceptual quality with only 0.39-1.88 going up in FID scores and imperceptible distortions in produced samples.

4.3. Text-guided Image Generation

In this section, we evaluate Q-Diffusion on Stable Diffusion pretrained on subsets of 512×512 LAION-5B for text-guided image generation. Inspired by [34], we sample text prompts from the MS-COCO [25] dataset and include them in the inputs of Algorithm 1 to generate a calibration dataset with texts condition. In this work, we fix the guidance strength to the default 7.5 in Stable Diffusion as the trade-off between sample quality and diversity. Qualitative results are

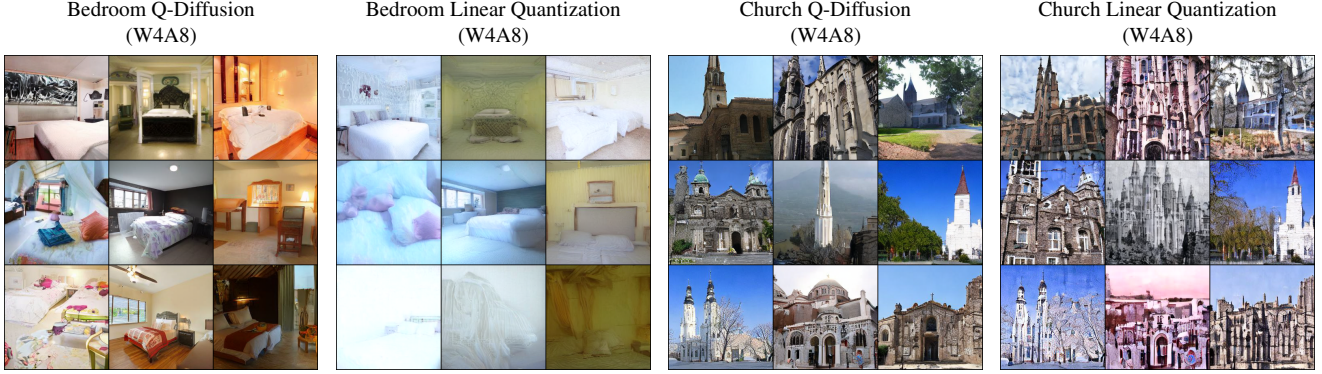


Figure 4: 256×256 unconditional image generation results using Q-Diffusion and Linear Quantization under W4A8 precision.

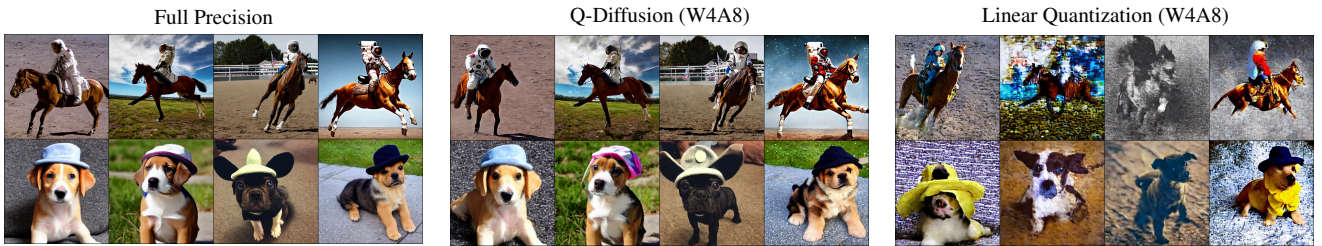


Figure 5: Stable Diffusion 512×512 text-guided image synthesis results using Q-Diffusion and Linear Quantization under W4A8 precision.

Table 2: Quantization results for unconditional image generation with DDIM on CIFAR-10 (32×32).

Model	Method	Bits (W/A)	FID↓	IS↑
DDIM	Baseline	32/32	4.22	9.12
	Linear Quant	8/32	4.71	8.93
	Q-Diffusion	8/32	4.34	9.15
	Linear Quant	4/32	141.47	4.20
	Q-Diffusion	4/32	5.06	8.86
	Linear Quant	8/8	14.00	8.89
	Q-Diffusion	8/8	4.24	9.42
	Linear Quant	4/8	72.31	5.96
	Q-Diffusion	4/8	5.07	9.13

shown in Figure 5. Compared to Linear Quantization, our Q-Diffusion provides higher-quality images with more realistic details and better reflections of the semantic information. The output of the W4A8 Q-Diffusion model largely resembles the output of the full precision model. Interestingly, we find some diversity in the lower-level semantics between the Q-Diffusion model and the FP models, like the heading of the horse or the shape of the hat. Understanding how

Table 3: Quantization results for unconditional image generation with LDM on LSUN-Bedrooms (256×256). The downsampling factor for the latent space is 4.

Model	Method	Bits (W/A)	FID↓
LDM-4	Baseline	32/32	2.98
	Linear Quantization	8/32	3.02
	Q-Diffusion	8/32	2.97
	Linear Quantization	4/32	82.69
	Q-Diffusion	4/32	4.86
	Linear Quantization	8/8	4.04
	Q-Diffusion	8/8	3.63
	Linear Quantization	4/8	54.10
	Q-Diffusion	4/8	4.55

quantization contributes to this diversity shall be explored in the future.

5. Related Work

Several approaches have been proposed to improve the efficiency and effectiveness of the diffusion process, which

Table 4: Quantization results for unconditional image generation with LDM on LSUN-Churches (256×256). The downsampling factor for the latent space is 8.

Model	Method	Bits (W/A)	FID↓
LDM-8	Baseline	32/32	4.06
	Linear Quantization	8/32	3.84
	Q-Diffusion	8/32	4.03
	Linear Quantization	4/32	32.54
	Q-Diffusion	4/32	4.45
	Linear Quantization	8/8	4.18
	Q-Diffusion	8/8	4.26
	Linear Quantization	4/8	32.06
	Q-Diffusion	4/8	4.46

mainly focus on finding faster sampling strategies from sample trajectory learning. Related approaches that fall into this line of work include faster step size schedules for VP diffusions [7, 33], the incorporation of implicit phases in the denoising process [41], and analytical approximations to simplify the generation process [1, 27, 28]. There is also work that progressively distills diffusion to a student model that requires fewer time steps to provide the same quality images [38], which achieved relatively good results, but involved extremely expensive retraining procedures.

6. Conclusion

This work studies the use of quantization to accelerate diffusion models. We propose Q-Diffusion, a novel post-training quantization scheme that conducts calibration with multiple time steps in the diffusion models denoising computation, and achieves significant improvements in quantized model performance. Q-Diffusion models under 4-bit quantization achieve comparable results to the full precision models. In the future, we will investigate the optimal time steps importance sampling for the calibration process based on the property of the corresponding time step, utilize mixed-precision to further conduct ultra low-bit quantization, and implement customized integer CUDA kernels to measure real runtime speedup and memory reduction.

References

- [1] Fan Bao, Chongxuan Li, Jun Zhu, and Bo Zhang. Analyticdpm: an analytic estimate of the optimal reverse variance in diffusion probabilistic models. *ArXiv*, abs/2201.06503, 2022.
- [2] Yash Bhalgat, Jinwon Lee, Markus Nagel, Tijmen Blankevoort, and Nojun Kwak. Lsq+: Improving low-bit quantization through learnable offsets and better initialization. *2020 IEEE/CVF Conference on Computer Vision and Pattern Recognition Workshops (CVPRW)*, pages 2978–2985, 2020.
- [3] Andrew Brock, Jeff Donahue, and Karen Simonyan. Large scale gan training for high fidelity natural image synthesis. *arXiv preprint arXiv:1809.11096*, 2018.
- [4] Han Cai, Chuang Gan, and Song Han. Once for all: Train one network and specialize it for efficient deployment. *ArXiv*, abs/1908.09791, 2019.
- [5] Ruojin Cai, Guandao Yang, Hadar Averbuch-Elor, Zekun Hao, Serge J. Belongie, Noah Snively, and Bharath Hariharan. Learning gradient fields for shape generation. In *European Conference on Computer Vision*, 2020.
- [6] Yaohui Cai, Zhewei Yao, Zhen Dong, Amir Gholami, Michael W. Mahoney, and Kurt Keutzer. Zeroq: A novel zero shot quantization framework. *2020 IEEE/CVF Conference on Computer Vision and Pattern Recognition (CVPR)*, pages 13166–13175, 2020.
- [7] Nanxin Chen, Yu Zhang, Heiga Zen, Ron J. Weiss, Mohammad Norouzi, and William Chan. Wavegrad: Estimating gradients for waveform generation. *ArXiv*, abs/2009.00713, 2020.
- [8] Tim Dettmers, Mike Lewis, Younes Belkada, and Luke Zettlemoyer. Llm.int8(): 8-bit matrix multiplication for transformers at scale. *arXiv preprint arXiv:2208.07339*, 2022.
- [9] Prafulla Dhariwal and Alexander Nichol. Diffusion models beat gans on image synthesis. *Advances in Neural Information Processing Systems*, 34, 2021.
- [10] Zhen Dong, Zhewei Yao, Daiyaan Arfeen, Amir Gholami, Michael W Mahoney, and Kurt Keutzer. Hawq-v2: Hessian aware trace-weighted quantization of neural networks. *Advances in neural information processing systems*, 33:18518–18529, 2020.
- [11] Zhen Dong, Zhewei Yao, Amir Gholami, Michael W. Mahoney, and Kurt Keutzer. Hawq: Hessian aware quantization of neural networks with mixed-precision. *2019 IEEE/CVF International Conference on Computer Vision (ICCV)*, pages 293–302, 2019.
- [12] Steven K. Esser, Jeffrey L. McKinstry, Deepika Bablani, Rathinakumar Appuswamy, and Dharmendra S. Modha. Learned step size quantization. In *International Conference on Learning Representations*, 2020.
- [13] Amir Gholami, Sehoon Kim, Zhen Dong, Zhewei Yao, Michael W. Mahoney, and Kurt Keutzer. A survey of quantization methods for efficient neural network inference. *ArXiv*, abs/2103.13630, 2021.
- [14] Ian Goodfellow, Jean Pouget-Abadie, Mehdi Mirza, Bing Xu, David Warde-Farley, Sherjil Ozair, Aaron Courville, and Yoshua Bengio. Generative adversarial nets. *Advances in neural information processing systems*, 27, 2014.
- [15] Cong Guo, Yuxian Qiu, Jingwen Leng, Xiaotian Gao, Chen Zhang, Yunxin Liu, Fan Yang, Yuhao Zhu, and Minyi Guo. Squant: On-the-fly data-free quantization via diagonal hessian approximation. *ArXiv*, abs/2202.07471, 2022.
- [16] Martin Heusel, Hubert Ramsauer, Thomas Unterthiner, Bernhard Nessler, and Sepp Hochreiter. Gans trained by a two time-scale update rule converge to a local nash equilibrium. *Advances in neural information processing systems*, 30, 2017.
- [17] Jonathan Ho, Ajay Jain, and Pieter Abbeel. Denoising diffusion probabilistic models. *Advances in Neural Information Processing Systems*, 33:6840–6851, 2020.

- [18] Tero Karras, Miika Aittala, Janne Hellsten, Samuli Laine, Jaakko Lehtinen, and Timo Aila. Training generative adversarial networks with limited data. *Advances in Neural Information Processing Systems*, 33:12104–12114, 2020.
- [19] Tero Karras, Samuli Laine, and Timo Aila. A style-based generator architecture for generative adversarial networks. In *Proceedings of the IEEE/CVF conference on computer vision and pattern recognition*, pages 4401–4410, 2019.
- [20] Tero Karras, Samuli Laine, Miika Aittala, Janne Hellsten, Jaakko Lehtinen, and Timo Aila. Analyzing and improving the image quality of stylegan. In *Proceedings of the IEEE/CVF conference on computer vision and pattern recognition*, pages 8110–8119, 2020.
- [21] Diederik P Kingma and Max Welling. Auto-encoding variational bayes. *stat*, 1050:1, 2014.
- [22] Alex Krizhevsky et al. Learning multiple layers of features from tiny images. 2009.
- [23] Haoying Li, Yifan Yang, Meng Chang, Huajun Feng, Zhi hai Xu, Qi Li, and Yue ting Chen. Srdiff: Single image super-resolution with diffusion probabilistic models. *Neuro-computing*, 479:47–59, 2021.
- [24] Yuhang Li, Ruihao Gong, Xu Tan, Yang Yang, Peng Hu, Qi Zhang, Fengwei Yu, Wei Wang, and Shi Gu. {BRECQ}: Pushing the limit of post-training quantization by block reconstruction. In *International Conference on Learning Representations*, 2021.
- [25] Tsung-Yi Lin, Michael Maire, Serge J. Belongie, James Hays, Pietro Perona, Deva Ramanan, Piotr Dollár, and C. Lawrence Zitnick. Microsoft coco: Common objects in context. In *European Conference on Computer Vision*, 2014.
- [26] Yijiang Liu, Huanrui Yang, Zhen Dong, Kurt Keutzer, Li Du, and Shanghang Zhang. Noisyquant: Noisy bias-enhanced post-training activation quantization for vision transformers. *arXiv preprint arXiv:2211.16056*, 2022.
- [27] Cheng Lu, Yuhao Zhou, Fan Bao, Jianfei Chen, Chongxuan Li, and Jun Zhu. Dpm-solver: A fast ode solver for diffusion probabilistic model sampling in around 10 steps. *ArXiv*, abs/2206.00927, 2022.
- [28] Cheng Lu, Yuhao Zhou, Fan Bao, Jianfei Chen, Chongxuan Li, and Jun Zhu. Dpm-solver++: Fast solver for guided sampling of diffusion probabilistic models. *ArXiv*, abs/2211.01095, 2022.
- [29] Calvin Luo. Understanding diffusion models: A unified perspective. *arXiv preprint arXiv:2208.11970*, 2022.
- [30] Markus Nagel, Rana Ali Amjad, Mart van Baalen, Christos Louizos, and Tijmen Blankevoort. Up or down? adaptive rounding for post-training quantization. *ArXiv*, abs/2004.10568, 2020.
- [31] Chenhao Niu, Yang Song, Jiaming Song, Shengjia Zhao, Aditya Grover, and Stefano Ermon. Permutation invariant graph generation via score-based generative modeling. In *International Conference on Artificial Intelligence and Statistics*, 2020.
- [32] Aditya Ramesh, Prafulla Dhariwal, Alex Nichol, Casey Chu, and Mark Chen. Hierarchical text-conditional image generation with clip latents. *arXiv preprint arXiv:2204.06125*, 2022.
- [33] Robin San Roman, Eliya Nachmani, and Lior Wolf. Noise estimation for generative diffusion models. *ArXiv*, abs/2104.02600, 2021.
- [34] Robin Rombach, A. Blattmann, Dominik Lorenz, Patrick Esser, and Björn Ommer. High-resolution image synthesis with latent diffusion models. *2022 IEEE/CVF Conference on Computer Vision and Pattern Recognition (CVPR)*, pages 10674–10685, 2021.
- [35] Chitwan Saharia, William Chan, Saurabh Saxena, Lala Li, Jay Whang, Emily Denton, Seyed Kamyar Seyed Ghasemipour, Burcu Karagol Ayan, S Sara Mahdavi, Rapha Gontijo Lopes, et al. Photorealistic text-to-image diffusion models with deep language understanding. *arXiv preprint arXiv:2205.11487*, 2022.
- [36] Chitwan Saharia, Jonathan Ho, William Chan, Tim Salimans, David J. Fleet, and Mohammad Norouzi. Image super-resolution via iterative refinement. *IEEE transactions on pattern analysis and machine intelligence*, PP, 2021.
- [37] Tim Salimans, Ian Goodfellow, Wojciech Zaremba, Vicki Cheung, Alec Radford, and Xi Chen. Improved techniques for training gans. *Advances in neural information processing systems*, 29, 2016.
- [38] Tim Salimans and Jonathan Ho. Progressive distillation for fast sampling of diffusion models. *ArXiv*, abs/2202.00512, 2022.
- [39] Hiroshi Sasaki, Chris G. Willcocks, and T. Breckon. Unit-ddpm: Unpaired image translation with denoising diffusion probabilistic models. *ArXiv*, abs/2104.05358, 2021.
- [40] Maying Shen, Hongxu Yin, Pavlo Molchanov, Lei Mao, Jianna Liu, and Jose Alvarez. Structural pruning via latency-saliency knapsack. In *Advances in Neural Information Processing Systems*, 2022.
- [41] Jiaming Song, Chenlin Meng, and Stefano Ermon. Denoising diffusion implicit models. *arXiv preprint arXiv:2010.02502*, 2020.
- [42] Yang Song and Stefano Ermon. Generative modeling by estimating gradients of the data distribution. *Advances in Neural Information Processing Systems*, 32, 2019.
- [43] Yang Song, Jascha Sohl-Dickstein, Diederik P Kingma, Abhishek Kumar, Stefano Ermon, and Ben Poole. Score-based generative modeling through stochastic differential equations. *arXiv preprint arXiv:2011.13456*, 2020.
- [44] Di Wu, Qingming Tang, Yongle Zhao, Ming Zhang, Ying Fu, and Debing Zhang. Easyquant: Post-training quantization via scale optimization. *ArXiv*, abs/2006.16669, 2020.
- [45] Lirui Xiao, Huanrui Yang, Zhen Dong, Kurt Keutzer, Li Du, and Shanghang Zhang. Csq: Growing mixed-precision quantization scheme with bi-level continuous sparsification. *arXiv preprint arXiv:2212.02770*, 2022.
- [46] Minkai Xu, Lantao Yu, Yang Song, Chence Shi, Stefano Ermon, and Jian Tang. Geodiff: a geometric diffusion model for molecular conformation generation. *ArXiv*, abs/2203.02923, 2022.
- [47] Huanrui Yang, Lin Duan, Yiran Chen, and Hai Li. Bsq: Exploring bit-level sparsity for mixed-precision neural network quantization. *ArXiv*, abs/2102.10462, 2021.

- [48] Huanrui Yang, Hongxu Yin, Pavlo Molchanov, Hai Li, and Jan Kautz. Nvit: Vision transformer compression and parameter redistribution. *ArXiv*, abs/2110.04869, 2021.
- [49] Zhewei Yao, Zhen Dong, Zhangcheng Zheng, Amir Gholami, Jiali Yu, Eric Tan, Leyuan Wang, Qijing Huang, Yida Wang, Michael Mahoney, et al. Hawq-v3: Dyadic neural network quantization. In *International Conference on Machine Learning*, pages 11875–11886. PMLR, 2021.
- [50] Fisher Yu, Ari Seff, Yinda Zhang, Shuran Song, Thomas Funkhouser, and Jianxiong Xiao. Lsun: Construction of a large-scale image dataset using deep learning with humans in the loop. *arXiv preprint arXiv:1506.03365*, 2015.
- [51] Shuchang Zhou, Zekun Ni, Xinyu Zhou, He Wen, Yuxin Wu, and Yuheng Zou. Dorefa-net: Training low bitwidth convolutional neural networks with low bitwidth gradients. *ArXiv*, abs/1606.06160, 2016.

A. Extended Experimental Settings

A.1. Implementation Details

We describe the implementation and compute details of the experiments in this section. We adapt the official implementation for DDIM [41]¹ and Latent Diffusion [34]². For Stable Diffusion, we use the CompVis codebase³ and its v1.4 checkpoint. We use the torch-fidelity library⁴ to evaluate FID and IS scores as done in [34].

For quantization experiments, we quantize all weights and activations, but leave activation functions and attention matrix multiplications running with full precision. As demonstrated in Appendix B, we always disable activation quantization for the first three Conv layers with residual connections and use INT8 precision in DDIM experiments on CIFAR-10 as activations of them present as exceedingly large outliers. No special modifications or mixed precision are done for other experiments.

A.2. Hyperparameters

Here we provide the hyperparameters used for our Q-Diffusion calibration in Table 5.

Experiment	T	c	n	N
DDIM CIFAR-10	100	5	256	5120
LDM-4 LSUN-Bedroom	200	10	256	5120
LDM-8 LSUN-Church	500	25	256	5120
Stable Diffusion	50	2	256	6400

Table 5: Hyperparameters for each experiment, including the number of denoising time steps T , intervals for sampling calibration data c , amount of calibration data per sampling step n , and the total number of calibration data N

B. Layer-wise Activations Distribution in DDIM and LDM

We study the distribution of activation values across all time steps in DDIM on CIFAR-10 and LDM on LSUN-Church. Figure 6 shows that the first three Conv layers with residual connections in DDIM have much larger activation ranges that go up to around 600-1200, while these ranges for the majority layers are < 50 . On the other hand, all layers in LDM share relatively uniform activation distribution, having a range < 15 .

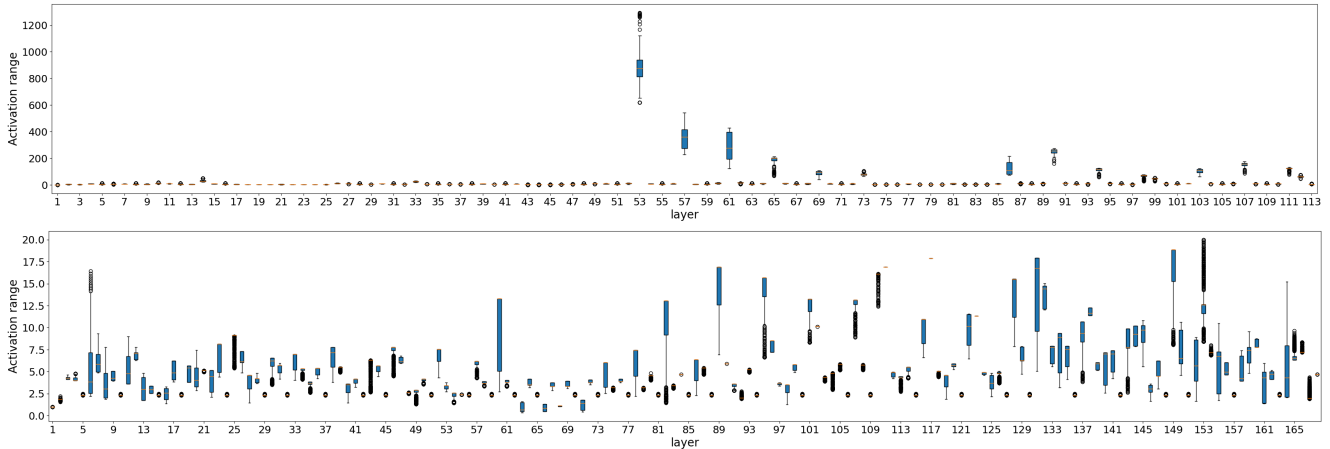


Figure 6: Activation ranges of FP32 outputs across layers averaging among all time steps. (Up) DDIM (Bottom) LDM

¹<https://github.com/ermongroup/ddim>

²<https://github.com/CompVis/latent-diffusion>

³<https://github.com/CompVis/stable-diffusion>

⁴<https://github.com/toshas/torch-fidelity>

C. Additional Random Samples

In this section, we provide our non-cherry-picked samples from our weight-only quantized and fully quantized diffusion models obtained using Q-Diffusion under 4-bit quantization. Results are shown in the figures below.

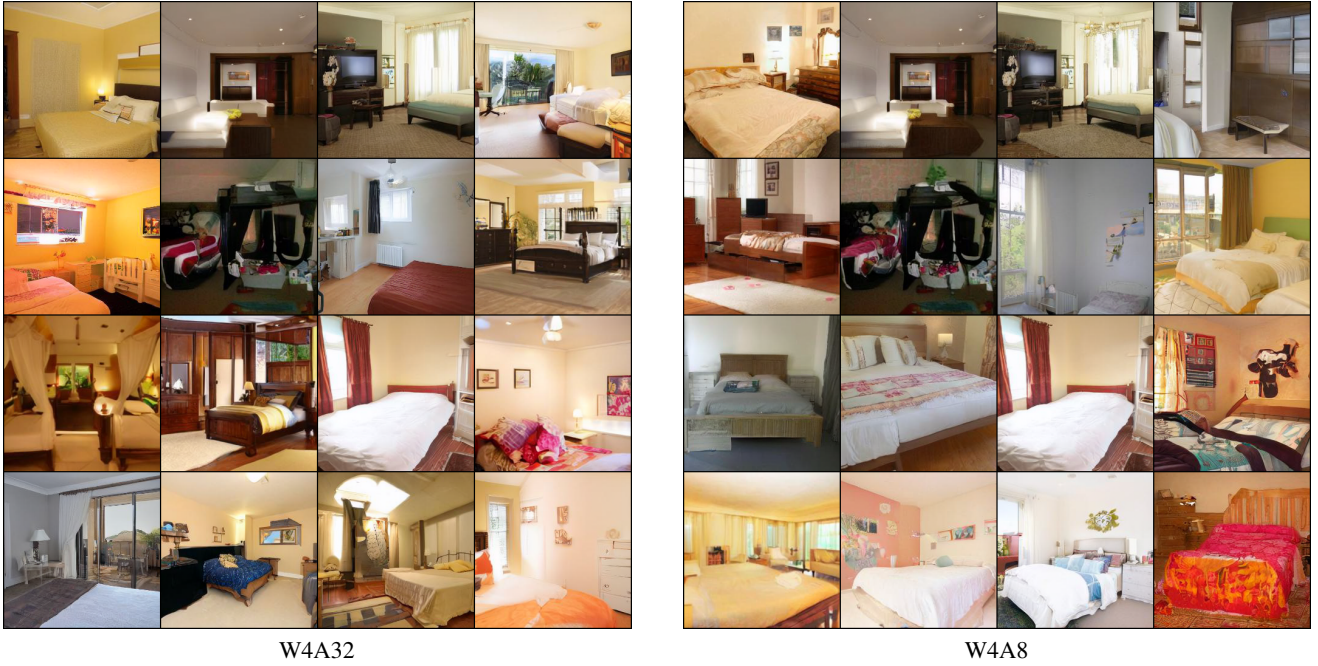


Figure 7: Random samples from our INT4 quantized 256×256 LSUN-Bedroom models with a fixed random seed.



Figure 8: Random samples from our INT4 quantized 256×256 LSUN-Church models with a fixed random seed.

Prompt: “Cluttered house in the woods in anime oil painting style.”



W4A32



W4A8

Prompt: “A puppy wearing a hat.”



W4A32



W4A8

Figure 9: Text-guided image generation on 512×512 LAION-5B from our INT4 quantized Stable Diffusion model with a fixed random seed.